Solid State Communications 249 (2017) 24–29

Contents lists available at ScienceDirect

Solid State Communications

journal homepage: www.elsevier.com/locate/ssc

Communication

First-principles calculations of hydrogen in perfect WFe and WFeNb crystals

L. Chen[a,*], Q. Wang[a], L. Xiong[a], H.R. Gong[b]

[a] Key Laboratory for Microstructural Control of Metallic Materials of Jiangxi Province, Nanchang Hangkong University, Nanchang, Jiangxi 330063, China
[b] State Key Laboratory of Powder Metallurgy, Central South University, Changsha, Hunan 410083, China

ARTICLE INFO

Keywords:
A. WFeH phases
A. WFeNbH phases
C. Mechanical properties
D. Diffusion of H

ABSTRACT

First principles calculations reveal that the addition Nb in WFeH phases changes the preferred site, i.e., WFeH(O2) → WFeNbH(T), and the addition of Nb can decrease the structural stability of WFeNbH(T) phase. It is also shown that Nb-H bond should have a stronger chemical bonding than W-H bond and Fe-H bond in WFeNbH phases when the bond length is bigger than 1.8 Å, which account for favorable mechanical properties of WFeNbH phases. Additionally, the most probable paths of H diffusion in WFe and WFeNb phases are calculated. The values of barriers denote that the addition of Nb in WFeH phases can result in H diffusing rapidly. The calculated results are in good agreements with experimental observations in the literature, and are discussed in terms of electronic structures and bond characteristics.

1. Introduction

During the past years, the binary system of W-Fe has been not only commonly regarded as armor materials or coating materials [1,2], but also as a potential candidate for plasma facing components (PFC) in fusion reactors, mainly due to its superior properties such as sufficient ductility, high melting temperature, high strength, low sputtering yield, and low hydrogen solubility, etc. [3–7]. Theory possibility of BCC WFe phases have been investigated by both experimental and calculation methods [8–14]. Moreover, in the aspect of application in fusion reactors, hydrogen (H) and its isotopes in perfect WFe crystal have important effects [15–18]. Accordingly, interest on this aspect has undergone a remarkable renaissance in recent years.

It has been reported that hydrogen at the tetrahedral site of BCC W_8Fe_8 is energetically unstable and will relax to the octahedral site, which is quite different from the preferred tetrahedral site of BCC W [18]. In this regard, as part of our continuing research the effects of H on structural stability and magnetic properties of WFe phases, in this study, the effects of H on mechanical properties and diffusion behaviors of WFe phases were investigated systematically by first-principles calculations. More importantly, niobium (Nb) has been well regarded as one of the highest hydrogen permeability materials, and recent researches have provided strong supports that the strength of W/Fe joint has been improved by niobium (Nb) in the experimental methods [19,20]. However, there is no study in the literature that reports the effects of H in perfect WFeNb crystals. Therefore, it is essential to investigate the comparison of various properties between WFeNbH and WFeH phases through calculation methods.

By means of highly accurate first principles calculations based on density functional theory, the present study is dedicated to systematically find out the fundamental effects of H on mechanical properties and diffusion behavior in perfect WFe and WFeNb crystals. It is worth noting that the WFe phase with equal atomic compositions of W and Fe is continuing to be selected as a typical example in present calculation [18]. The composition of 5 at% of Nb in WFe are also selected, as the composition is similar to the experimentally observed WFe-5%Nb phase with excellent capability of interface strength [19]. In addition, H behaviors in W bulk is also calculated for the sake of comparison. It will be shown that the derived results are not only in good agreement with experimental results, but also provide a deeper understanding on various properties of WH, WFeH and WFeNbH phases.

2. Theoretical methods

The first principles calculations are based on the well-established Vienna ab initio Simulation Package (VASP) with a plane wave basis and projector-augmented-wave (PAW) method [21,22]. A gradient corrected functional has been used to describe electronic exchange and correlations [23], and the cutoff energy is 400 eV for plane wave basis. During k space integration, the temperature smearing method of Methfessel–Paxton [24] is chosen for relaxation calculation and the modified tetrahedron method of Blöchl-Jepsen-Andersen [25] is

* Corresponding author.
E-mail address: clcl83@163.com (L. Chen).

http://dx.doi.org/10.1016/j.ssc.2016.10.013
Received 16 September 2016; Received in revised form 5 October 2016; Accepted 20 October 2016
Available online 27 October 2016

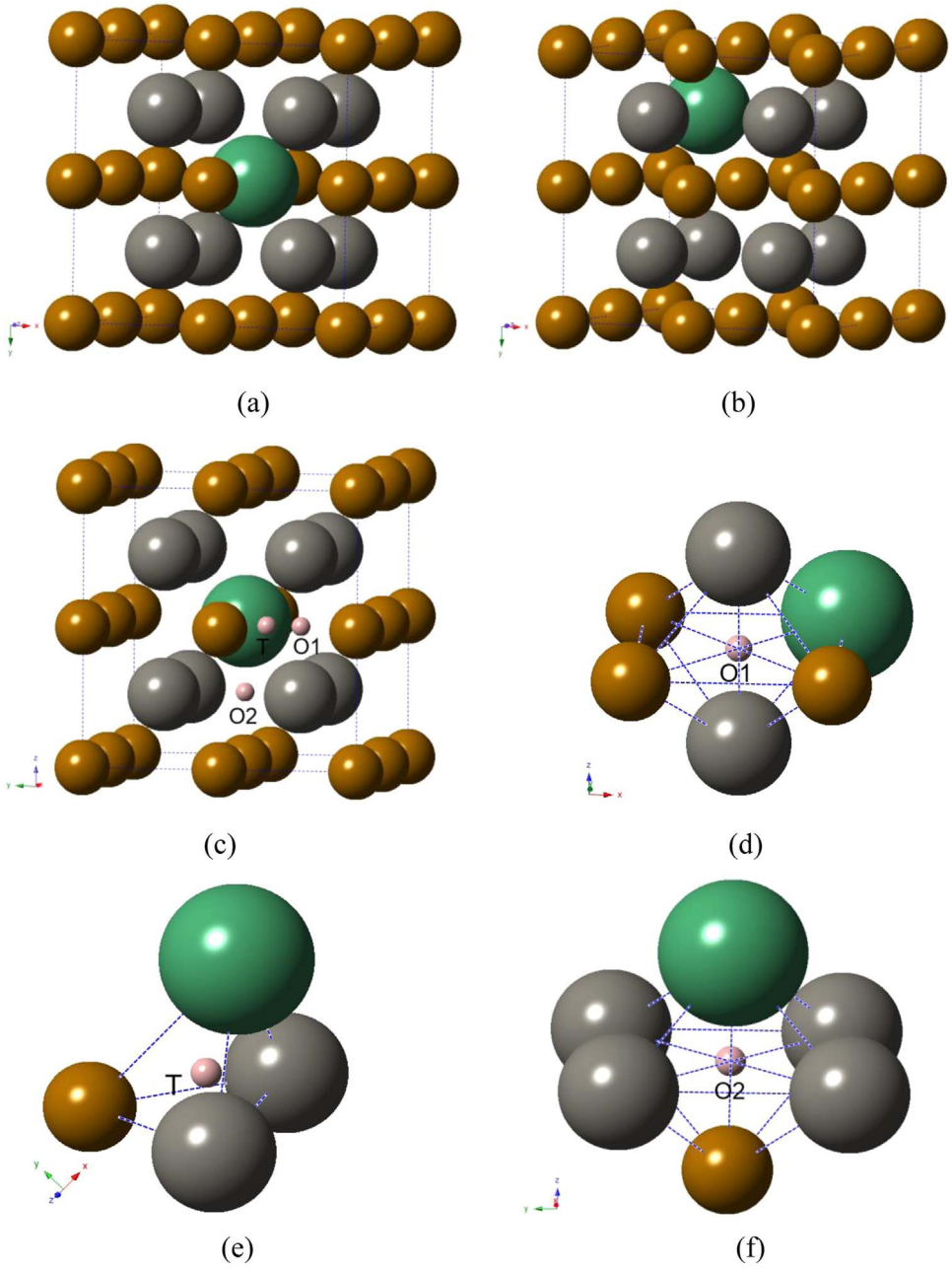

Fig. 1. Schematic illustrations of (a) W_8Fe_7Nb phase, (b) W_7Fe_8Nb phase, (c) various interstitial sites of W_8Fe_7Nb bulk, (d) octahedral (O1) site, (e) tetrahedral (T) site, and (f) octahedral (O2) site. The largest green, second largest gray, third largest yellow, and smallest red balls represent Nb, W, Fe, and H atoms, respectively. (For interpretation of the references to color in this figure legend, the reader is referred to the web version of this article.)

performed for static calculations. In each calculation, periodic boundary conditions are applied along three directions of the unit cell.

To calculate various properties in WFeH and WFeNbH crystals, a 2×2×2 (16 atoms) supercell with 9×9×9 and 11×11×11 k-mesh are selected for relaxation and static calculations, respectively, while 15×15×15 is selected for the calculations of density of states(DOS) and elastic constants. each calculation is employed to ensure the energy convergence within an error of 1 meV per atom. It should be noted that each calculation exhibits the ferromagnetic state for Fe overlayers.

To simulate the composition of WFe-5%Nb, one W or Fe atom of each unit cell is substituted by one Nb atom. As a typical example, Fig. 1 shows two kinds of WFeNb phases, Fig. 1(a) shows the W_8Fe_7Nb phase, and Fig. 1(b) shows the W_7Fe_8Nb phase. One H atom is then added, respectively, at the tetrahedral (T) and octahedral (O) sites of BCC W, WFe and WFeNb. Typical examples including schematic illustrations of W_8Fe_7NbH with T and O sites are shown through Fig. 1(c)–(f). It is worth noting that there are two kinds of O sites for W_8Fe_7Nb, i.e., O1 and O2 sites with different surrounding atoms of W, Fe, and Nb as shown obviously in Fig. 1(d) and (f).

3. Results and discussion

3.1. Solution energy

To investigate the effects of Nb on structural stability of WFeNb phases, the solution energy (E_{sol}) which one W or Fe atom is substituted by one Nb atom is calculated according to the following formula:

$$E_{sol} = E_{W_nFe_{n-1}Nb} - E_{W_nFe_n} - E_{Nb} + E_{Fe}, \quad (1)$$

$$E_{sol} = E_{W_{n-1}Fe_nNb} - E_{W_nFe_n} - E_{Nb} + E_W, \quad (2)$$

where $E_{W_nFe_{n-1}Nb}$, $E_{W_{n-1}Fe_nNb}$, $E_{W_nFe_n}$, ENb, EF$_e$ and E_W are total energies of $W_nFe_{n-1}Nb$, $W_{n-1}Fe_nNb$, W_nFe_n, pure Nb, pure W and pure Fe, respectively. After the calculations, the present E_{sol} of W_8Fe_7Nb and W_7Fe_8Nb are −0.116 and −0.207 eV, respectively. As both W_8Fe_7Nb and W_7Fe_8Nb, the E_{sol} of a unit cell(16 atoms) with negative values is so close to each other, i.e., the W_8Fe_7Nb and W_7Fe_8Nb are also energetically possible to exist. Moreover, the addition W in Nb improve the resistance to hydrogen embrittlement by experimental methods [26]. Therefore, as a typical example, the W_8Fe_7Nb with more W-Nb bonds will be purposely selected in the next calculation.

We turn to investigate the effects of H on structural stability of W_8Fe_7NbH phase. The zero-point energy (*ZPE*) correction is calculated by means of the harmonic approximation:

$$\overline{E_j}(T) \approx \frac{1}{2}\hbar\omega_j + \frac{\hbar\omega_j e^{-\hbar\omega_j/k_BT}}{1 - e^{-\hbar\omega_j/k_BT}} = \frac{1}{2}\hbar\omega_j + \frac{\hbar\omega_j}{e^{\hbar\omega_j/k_BT} - 1}, \quad (3)$$

when the temperature T approaches zero, the above energy reaches its minimum value of $\frac{1}{2}\hbar\omega_j$, which is ZPE and could be represented as:

$$E_{ZPE} \approx \frac{1}{2}\sum_j \hbar\omega_j, \quad (4)$$

where ω_j is the frequency associated with the harmonic mode in the GAMMA point. To obtain the *ZPE* in the present study, the metal atoms of W, Fe and Nb are kept immobile and the H atom is relaxed only, due to the huge differences of frequencies between H and W, Fe and Nb.

The E_{sol} of one H atom in W_8Fe_7NbH phase without the consideration of *ZPE* of H is calculated by means of the following formula:

$$E_{sol} = E_{WFeNbH} - E_{WFeNb} - E_H, \quad (5)$$

and the corresponding E_{sol} with *ZPE* are derived as follows:

$$E_{sol} = E_{WFeNbH} + E^{ZP}_{WFeNbH} - E_{WFeNb} - E_H - E^{ZP}_H, \quad (6)$$

where E_{WFeNbH} is total energies of W_8Fe_7NbH phase, E_{WFeNb} is corresponding to total energies of W_8Fe_7Nb bulk before H addition, and E_H is total energy of H atom in a H_2 molecule. E^{ZP}_{WFeNbH} is *ZPE* of H in W_8Fe_7NbH phase, and $E^{ZP}_H$is *ZPE* of H in the H_2 molecule. It is should be pointed out that the calculated *ZPE* (0.26 eV) of H atom in H_2 is in excellent agreement with 0.27 eV from the other work [27]. After the calculations, the *ZPE* and E_{sol} of H in W_8Fe_7NbH phase are derived and the results are summarized in Table 1.

Firstly, several features could be observed from Table 1. The *ZPE* value of H in T site of W_8Fe_7Nb is bigger than that in the corresponding O site, suggesting that the stable sites of W_8Fe_7Nb possess higher vibrating frequency of H. Moreover, one can also discern from Table 1 that the inclusion of *ZPE* does not change the most stable site of W_8Fe_7NbH phase, which is a similar observation in $W_{16}H$ or W_8Fe_8H phases [18,28]. All the above characteristics suggest that *ZPE* has a negligible effect on structural stability of W_8Fe_7NbH phase. In addition, the W_8Fe_7NbH(T) phase is energetically less favorable with higher E_{sol} value (0.349 eV) than the corresponding W_8Fe_8H(O2) phase (0.08 eV) [18], suggesting that the addition of Nb would decrease the solubility of H in the O2 site of W_8Fe_8.

Table 2
Comparison of bond lengths of the W-H, Fe-H and Nb-H bonds in the W_8Fe_7NbH phase before and after relaxations. The integer in the parenthesis after the bond length signifies the number of the bond.

Type	H location		W-H bond (Å)	Fe-H bond (Å)	Nb-H bond (Å)
W_8Fe_7NbH	T site	Before relaxation	1.703(2)	1.703(1)	1.703(1)
		After relaxation	1.863(2)	1.643(1)	1.933(1)
	O1 site	Before relaxation	1.523(2)	2.155(3)	2.155(1)
		After relaxation	1.814(2)	2.155(2); 2.212(1)	1.964(1)
	O2 site	Before relaxation	2.155(4)	1.523(1)	1.523(1)
		After relaxation	2.194(4)	1.547(1)	1.827(1)

In addition, for W_8Fe_7NbH phase, interestingly, the T site is energetically more favorable with lower E_{sol} (0.349 eV) than its corresponding O site (0.365 or 0.572 eV), which is quite different from W_8Fe_8 in the literature [18]. Accordingly, more about the T sites of W_8Fe_7NbH could be discussed in a little bit depth, and the bond lengths of the W-H, Fe-H and Nb-H bonds in the W_8Fe_7NbH phase before and after relaxations are derived and the results are listed in Table 2. For the T site, the H atom and four nearest bonds has formed the T site before relaxation, i.e., two W-H, one Fe-H and one Nb-H bonds with the same bond length of 1.730 Å. After the relaxation, the original bond length of the T site undergoes a large change, however, the amount of bonds at T site in W_8Fe_7NbH phase remains unchanged. It therefore follows that the T site of W_8Fe_7NbH phase is stable, which is as the same as the stable T site of pure W as related before. One conclusion from this section is that the addition of Nb can change the preferred site in W_8Fe_8H phase, i.e., W_8Fe_8H(O2) →W_8Fe_7NbH(T). (Table 3).

3.2. Mechanical properties

It is interesting to find out the influence of H on mechanical properties in perfect crystals, and the elastic constants of W, WH, W_8Fe_8H and W_8Fe_7NbH phases are derived through the process of the minimization of total energies. The elastic constants (C_{11}, C_{12}, and C_{44}) are calculated through the strain-energy approach [29], and the elastic

Table 1
Elastic constants(C_{11}, C_{12}, C_{44}), bulk modulus(B), shear modulus(G), Youngs modulus(E), *ZPE* and E_{sol} for pure W, $W_{16}H$ phases, W_8Fe_8H phases, and W_8Fe_7NbH phases..

Phases	Type	C_{11}	C_{12}	C_{44}	B	G	E	*ZPE* (eV/atom)	E_{sol} (eV)	
									Without *ZPE*	With *ZPE*
W	This work	523.86	203.46	152.18	310.26	155.34	399.37			
	Exp.[a]	532.55	204.95	163.13	314.15	163.40	417.76			
$W_{16}H$ (T)	This work	507.69	202.67	134.34	304.34	141.34	367.17	0.262	1.02	1.022
$W_{16}H$ (O)	This work	501.30	182.78	124.20	303.06	124.02	327.40	0.15	1.395	1.285
W_8Fe_8H (O2)	This work	297.00	206.20	102.31	236.47	73.84	200.65	0.202	0.08	0.022
W_8Fe_8H (O1)	This work	286.59	194.84	97.25	216.14	71.93	194.25	0.131	0.76	0.631
W_8Fe_7NbH (T)	This work	305.95	207.75	103.16	240.48	76.58	207.69	0.23	0.379	0.349
W_8Fe_7NbH (O1)	This work	295.47	180.9	93.81	219.09	76.97	206.71	0.14	0.485	0.365
W_8Fe_7NbH (O2)	This work	305.11	209.02	99.56	241.05	74.32	202.17	0.143	0.689	0.572

[a] Ref. [31].

Table 3
Migration barrier of H Diffusion along various paths in W, W_8Fe_8 and W_8Fe_7Nb phases..

No	Type	Diffusion direction	Migration barrier (eV)
1	This work	W(T)→W(T)	0.197
	Cal.		0.2[a]
2	This work	W_8Fe_8(O2)→W_8Fe_8(O2)	0.598
3	This work	W_8Fe_7Nb(T)→W_8Fe_7Nb(T)	0.193
4	This work	W(T)→W(O)	0.393
	Exp.		0.39[b]
5	This work	W_8Fe_8(O2)→W_8Fe_8(O1)	0.599
6	This work	W_8Fe_7Nb(T)→W_8Fe_7Nb(O2)	0.398
7	This work	W_8Fe_7Nb(T)→W_8Fe_7Nb(O1)	0.142

[a] Ref. [34].
[b] Ref. [28].

moduli (B, G, and E) are derived by means of the Voigt-Reuss-Hill's approximation [30]. After a series of calculations, Table 1 lists the derived elastic constants (C_{11}, C_{12} and C_{44}) and elastic moduli (B, G and E) of several phases, as well as available experimental results regarding the elastic constants of W bulk in the literature [31]. The C_{11}, C_{12}, and C_{44} of pure BCC W are calculated to be 523.86, 203.46, and 152.18 GPa, respectively, which fit well with the values of 532.55, 204.95, and 163.18 GPa from experimental values in the literature [31]. One can also see from Table 1 that the derived B, G and E of W are in general agreement with the corresponding data from experimental method [31].

Firstly, to provide insight into the elastic moduli details involved in the mechanical properties, the comparison data is listed in Table 1. The B, G, and E values of WH(T) and WH(O) phases are bigger than those of the corresponding W_8Fe_8H(O2) and W_8Fe_8H(O1) phases, respectively, suggesting that the addition of Fe could decrease the mechanical properties of WH phases. More importantly, it can be found out that the B, G, and E values of W_8Fe_7NbH(T) and W_8Fe_7NbH(O) phases are bigger than those of the corresponding W_8Fe_8H(O2) and W_8Fe_8H(O1) phases, respectively, suggesting that the addition of Nb can improve the mechanical properties of W_8Fe_8H phase.

Consequently, it is of interest to understand mechanical properties at bond characteristics of W_8Fe_8H and W_8Fe_7NbH phases. The bond energies of W_8Fe_8H and W_8Fe_7NbH phases can be calculated via the dimer method with a big cubic box (30×30×30 Å) [32], and the derived results are shown in Fig. 2 as a function of bond length. Therefore, the total bond energies of H atom in W, W_8Fe_8 and W_8Fe_7Nb crystals are thus derived, respectively. As a typical example of W_8Fe_8H(O1), W_8Fe_7NbH(O2) and W_8Fe_7NbH(O1), the total bond energies are calculated to be −13.3 [18], −13.832 and −13.323 eV after the relaxation, respectively. The comparison signifies that the least preferred site of W_8Fe_7NbH phase should have a stronger bonding with lower total bond energy. More importantly, it can be also observed from Fig. 2 that the bond energy of Nb-H at a certain bond length is much lower than that of the W-H bond and Fe-H bond when the bond length is bigger than 1.8 and 1.5 Å. Such a characteristic of bond energy will intrinsically improve the mechanical properties of W_8Fe_7NbH phases as related before.

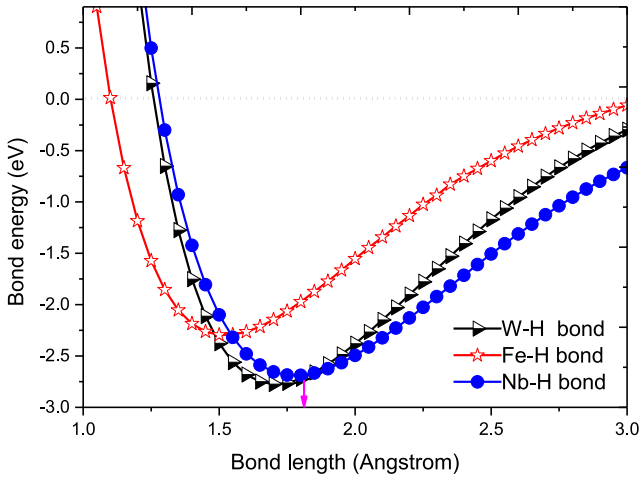

Fig. 2. Bond energies of W-H, Fe-H and Nb-H bonds as a function of bond length.

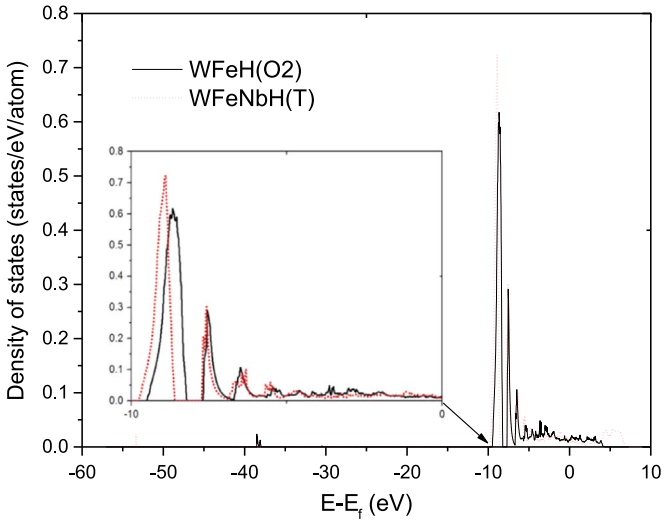

Fig. 3. Comparison of total density of states of hydrogen atom in W_8Fe_8(O2) and W_8Fe_7Nb(T) phases.

Furthermore, to have a further understanding of mechanical properties at an electronic scale, and the electronic structures of $W_{16}H$, W_8Fe_8H and W_8Fe_7NbH phases are thus calculated and compared with each other. As a typical example, Fig. 3 summarizes the comparison of total density of states (DOS) of H atoms in W_8Fe_8H(O2) and W_8Fe_7NbH(T) phases. Compared with those of the W_8Fe_8H(O2) phase, the DOS of W_8Fe_7NbH(T) below the Fermi level (E_f) have moved leftward to the positions with a little bigger binding energies, and the DOS peaks at about −8 eV below E_f are much higher. The above characteristics of electronic structures imply that the H atom has formed a stronger bonding in W_8Fe_7NbH(T) than that in W_8Fe_8H(O2), which is also in excellent agreement with the bond energies in Fig. 2.

3.3. Diffusion of H in crystals

The diffusion of H atoms is commonly regarded as a fundamental step during the process of fusion reactors of face plasma materials. As related before, there has not been any previous research regarding hydrogen diffusion of WFe and WFeNb in the literature. A comparative study of hydrogen diffusion in various W, W_8Fe_8 and W_8Fe_7Nb phases is therefore conducted in the present study, in order to find the influence of Nb and Fe on hydrogen diffusion of W_8Fe_8 and W, respectively.

For diffusion of H in the W, W_8Fe_8, W_8Fe_7Nb phases, the climbing image nudged elastic band method (cNEB) [33] is used to calculate the corresponding diffusion paths, and several intermediate states are generated by a linear interpolation method so as to find the migration barrier for diffusion process of H in interstitial site. During all the structural relaxation in this work, the total energy was converged to 10^{-5} eV in the electronic self-consistency loop and the maximum force criterion on each atom was 0.02 eV Å^{-1}. After a series of calculation, Table 2 lists energy barrier of H Diffusion along various paths in W, W_8Fe_8 and W_8Fe_7Nb phases, and Fig. 4 shows the derived migration barrier of several diffusion paths as typical examples. It should be noticed that the most probable paths of H diffusion between T and O

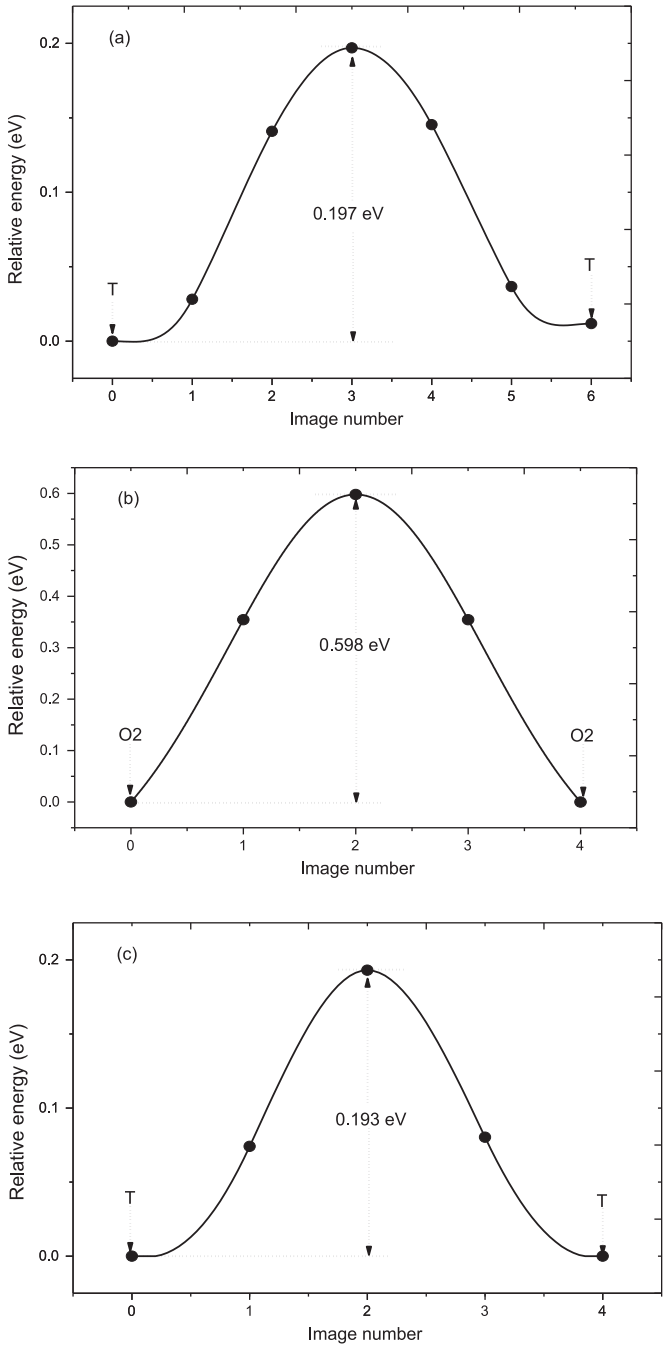

Fig. 4. Migration barrier of H diffusion from T to T in (a) W, (c) W_8Fe_7Nb and from O2 to O2 in (b) W_8Fe_8.

are considered, i.e., from T to T, from T to O (W, W_8Fe_7Nb) and from O to O (W_8Fe_8).

Several features could be derived from Table 2 and Fig. 4. Firstly, the present migration barrier of H in W bulk are calculated to be 0.197 and 0.393 eV, which are consistent with the corresponding values of 0.2 [34] and 0.39 eV [28] from computational results and experimental measurements. For diffusion of H in W bulk, the migration barrier through T is 0.197 eV, which is much lower than the corresponding values of 0.393 eV, implying that the diffusion path of H in W bulk should be mainly through T instead of O. Such a small energy barrier of 0.197 eV is also consistent with the rapid diffusion of H in W observed experimentally [28].

Secondly, we turn to find out H diffusion of W_8Fe_8 phase. One can deduce from Table 2 and Fig. 4 that migration barrier of H in W_8Fe_8 phase is calculated to be 0.598 and 0.599 eV through O1 and O2. Interestingly, the values of migration barrier is so closely in W_8Fe_8 phase, suggesting that the H diffusion paths from O2 to O2 or from O2 to O1 would be also energetically possible. In addition, one could perceive clearly from Fig. 4 that the migration barrier through O2 is higher than the corresponding T in W, and a similar observation can be seen through O site. The above suggests that the addition of Fe in W could make the H diffusion harder with higher migration barrier.

Thirdly, as to the diffusion of H in W_8Fe_7Nb phase, one can detect clearly from Table 2 that the migration barrier through T (0.193 eV) is smaller than the corresponding value O2 (0.398 eV). Interestingly, the migration barrier (0.193 eV) through T in W_8Fe_7Nb is higher than that through O1 (0.142 eV). Such close values of migration barrier to suggest that the diffusion path of H in W_8Fe_7Nb phases should be mainly two paths, i.e., T→O1 and T→T. More importantly, the migration barrier of H diffusion in W_8Fe_7Nb phases is much lower than those though O2 sites in W_8Fe_8 phase as well as through O1 sites. The above comparisons signify that the addition of Nb in W_8Fe_8H phase can make the H diffuse more easily because of smaller energy barrier and more diffusion paths. However, the migration barrier of T site in W_8Fe_7NbH phases (0.193 eV) seems to be lower than that of T site in W (0.197 eV) and a similar observation can be seen from O1 (0.142 eV) in W_8Fe_7NbH and O (0.393 eV) in W. These characteristics would account for the highest H diffusion and permeability in W_8Fe_7Nb phase.

4. Conclusions

First principles calculations based on density functional theory have been used to investigate the effects of H on structural stability, mechanical properties and H diffusion behavior of W_8Fe_8 and W_8Fe_7Nb phases. It is found that the addition of Nb could improve the mechanical properties of W_8Fe_8H phase, decrease the structural stability of W_8Fe_7NbH(T) phase, reduce the diffusion barrier of H, and increase diffusion paths for H. The calculated results are not only in excellent agreement with experimental observations in the literature [28,32], but also bring about fundamental explanations to the experimental evidence regarding in $W_{16}H$, W_8Fe_8H and W_8Fe_7NbH phases. In summary, the information obtained from this work will be useful to understand the mechanical properties and diffusion behavior of $W_{16}H$, W_8Fe_8H and W_8Fe_7NbH phases, and hopeful in the development of potential applications in PFC.

Acknowledgments

This research work was supported by Key Laboratory for Microstructural Control of Metallic Materials of Jiangxi Province (Grant No. JW201523003), National Natural Science Foundation of China (Grant No. 51463017).

References

[1] Y. Nishi, Y. Mogi, K. Oguri, T. Watanabe, J. Mater. Sci. Lett. 14 (1995) 1.
[2] H.B. Zhou, Y.L. Liu, S. Jin, Y. Zhang, G.N. Luo, G.H. Lu, Nucl. Fusion 50 (2010) 025016.
[3] M. Donten, H. Cesiulis, Z. Stojek, Electrochim. Acta 45 (2000) 3389.
[4] H. Leiva, K. Dwight, A. Wold, J. Solid State Chem. 42 (1982) 41.
[5] S.F. Huang, R.S. Chang, T.C. Leung, C.T. Chan, Phys. Rev. B 72 (2005) 075433.
[6] Y.L. Chiu, N. Baluc, R. Schäublin, Int. J. Mod. Phys. B 20 (2006) 4195.
[7] W.W. Basuki, J. Aktaa, J. Nucl. Mater. 417 (2011) 524.
[8] K. Sumiyama, M. Hirata, W. Teshima, Jpn. J. Appl. Phys. 30 (1991) 2839.
[9] U. Herr, K. Samwe, Nanostruct. Mater. 1 (1992) 515.
[10] E. Jartych, J.K. Żurawicz, D. Oleszak, M. Pekala, J. Magn. Magn. Mater. 18 (2002) 247.
[11] H.Y. Bai, C. Michaelsen, C. Gente, R. Bormann, Phys. Rev. B 63 (2001) 064202.
[12] A.A. Novakova, T.Y. Kiseleva, V.V. Lyovina, D.V. Kuznetsov, A.L. Dzidziguri, J. Alloy Compd. 317–18 (2001) 423.
[13] Y. Ruan, S. Yao, M. Kowaka, J. Non-Cryst. Solids 117/118 (1990) 752.
[14] Q.Q. Ren, J.L. Fan, Y. Han, H.R. Gong, J. Appl. Phys. 116 (2014) 093009.
[15] B.C. Odegard, B.A. Kalin, J. Nucl. Mater. 233–237 (1996) 44.

[16] S. Bagchi, S. Jani, S. Anwar, N. Lakshmi, N.P. Lalla, J. Magn. Magn. Mater. 322 (2010) 3851.
[17] H. Greuner, H. Bolt, B. Böswirth, S. Lindig, W. Kühnlein, T. Huber, K. Sato, S. Suzuki, Fusion Eng. Des. 75–79 (2005) 333.
[18] L. Chen, J.L. Fan, M. Song, H.R. Gong, Int. J. Hydrog. Energy 41 (2016) 13093.
[19] A. Ambroziak, M. Korzeniowski, P. Kustroń, M. Winnicki, Int. J. Refract. Met. Hard Mater. 29 (2011) 499.
[20] W.W. Basuki, J. Aktaa, Fusion Eng. Des. 86 (2011) 2585.
[21] G. Kresse, J. Hafner, Phys. Rev. B 47 (1993) 558.
[22] G. Kresse, J. Joubert, Phys. Rev. B 59 (1999) 1758.
[23] K. Govaerts, B. Partoens, D. Lamoen, Solid State Commun. 243 (2016) 36.
[24] M. Methfessel, A.T. Paxton, Phys. Rev. B 40 (1989) 3616.
[25] P.E. Blöchl, O. Jepsen, O.K. Andersen, Phys. Rev. B 49 (1994) 16223.
[26] N. Watanabe, H. Yukawa, T. Nambu, Y. Matsumoto, G.X. Zhang, M. Morinaga, J. Alloy. Comp. 477 (2009) 851.
[27] J.M. Rowe, J.J. Rush, L.A. de Graaf, G.A. Ferguson, Phys. Rev. Lett. 29 (1972) 1250.
[28] R. Frauenfelder, J. Vac. Sci. Technol. 6 (1969) 388.
[29] S.Q. Wang, H.Q. Ye, J. Phys. Condens. Matter 15 (2003) 5307.
[30] J.H. Westbrook, R.L. Fleischer, Intermetallic Compounds: basic Mechanical Properties and Lattice Defects of Intermetallic Compounds 2, Wiley, England, 2000, p. 10.
[31] F.H. Featherston, J. R. Neighb. Phys. Rev. 130 (1963) 1324.
[32] J.X. Yang, L. Chen, J.L. Fang, H.R. Gong, J. Alloy. Comp. 686 (2016) 160.
[33] H. Lin, Y.W. Wen, C.X. Zhang, L.L. Zhang, Y.H. Huang, B. Shan, R. Chen, Solid State Commun. 152 (2012) 999.
[34] Y.L. Liu, Y. Zhang, G.N. Luo, G.H. Lu, J. Nucl. Mater. 390–391 (2009) 1032.